

<https://doi.org/10.1038/s41524-024-01354-y>

Understanding and tuning negative longitudinal piezoelectricity in hafnia

Check for updates

Huirong Jing, Chaohong Guan & Hong Zhu

Most piezoelectric materials exhibit a positive longitudinal piezoelectric effect (PLPE), while a negative longitudinal piezoelectric effect (NLPE) is rarely reported or paid much attention. Here, utilizing first-principles calculations, we unveil the origin of negative longitudinal piezoelectricity in ferroelectric hafnia by introducing the concept of weighted projected bond strength around cation in the *c* direction (WPB_c), which is proposed to quantitatively characterize the asymmetric bonding stiffness along the strain direction. When the WPB_c is anti-parallel to the direction of bulk spontaneous polarization, the polarization decreases with respect to tensile strain and leads to a negative piezoelectricity. Furthermore, to confirm the influence of WPB_c on the piezoelectric effect and understand how the value of WPB_c influences the piezoelectric coefficient e_{33} , we acquire both the piezoelectric coefficient of doped hafnia and the corresponding bonding environment around each cation. The finding reveals that the more negative piezoelectric coefficient can be achieved through a concurrent achievement of the more negative average WPB_c and the lower standard deviation (STD) of WPB_c . In addition, the Sn-doped hafnia with the lowest average WPB_c and smaller STD- WPB_c is identified to have the highest piezoelectric coefficient (-2.04 C/m²) compared to other dopants, showing great potential in next-generation electromechanical devices.

Piezoelectric materials constitute a class of functional materials capable of converting energy between mechanical energy and electrical energy. Since the initial discovery of the piezoelectric effect in quartz by the Curie brothers in 1880¹, research on piezoelectric materials has thrived and found extensive applications in various fields, including medical ultrasound, sonar, sensors, vibration-powered electronics and more^{2–5}. Most piezoelectric materials exhibit positive longitudinal piezoelectricity, in which the polarization (*P*) increases with external tensile strain (ϵ) along the polar direction (Fig. 1a) and results in a positive piezoelectric coefficient e_{33} ($\partial P/\partial \epsilon$). In contrast, materials with negative longitudinal piezoelectricity are rarely reported. One well-known exception is the ferroelectric poly(vinylidene fluoride) (PVDF), where the polarization reduces with tensile strain in the polar direction (Fig. 1b), exhibiting negative longitudinal piezoelectricity^{6,7}. However, the origin of the negative longitudinal piezoelectric effect (NLPE) in PVDF has been attributed to the intermixed crystalline phase and no NLPE has been reported for a single phase. Besides, You et al. recently discovered the NLPE in the van der Waals layered ferroelectric CuInP_2S_6 in the experiment, which was attributed to the reduced lattice dimensionality⁸. In addition, several inorganic compounds have been theoretically predicted to possess NLPE^{9–11}. For example, Liu et al. demonstrate NLPE in several hexagonal ABC ferroelectrics, and Arora et al. report NLPE in 2D heterobilayers. It is

worth noting that almost all of the above structures are layered stacks with limited elastic constants¹², which can lead to significant mechanical losses and degraded performance for some electromechanical applications, such as high-frequency resonators, filters and ultrasonic motors.

Hafnia, a well-known high-*k* gate insulator, was first recognized for its ferroelectricity in silicon-doped thin films in 2011¹³. Since then, numerous researchers have dedicated their efforts to understanding the origin of ferroelectric behaviors in hafnia and exploring methods to control its ferroelectricity^{13–17}. Previous investigations have identified the ferroelectricity of hafnia originates from the polar orthorhombic phase (space group: $Pca2_1$)^{18–21}. Ferroelectric hafnia has now emerged as one of the most promising materials in the fields of electronic devices and storage applications^{13,22,23}. Interestingly, despite being a ferroelectric material, hafnia's electromechanical response, especially its piezoelectric properties, has received relatively little attention. However, due to its high mechanical strength, high speed of sound, and compatibility with CMOS²⁴, hafnia has the potential to serve as a candidate material for the piezoelectric bulk acoustic filter, offering an alternative to the widely used aluminum nitride (AlN). Recent first-principles studies predicted that ferroelectric hafnia presents the NLPE^{25,26}. However, the experimental measurement results of the longitudinal piezoelectricity of hafnia are still inconsistent. For example,

University of Michigan– Shanghai Jiao Tong University Joint Institute, Shanghai Jiao Tong University, Shanghai, 200240, China.

 e-mail: hong.zhu@sjtu.edu.cn

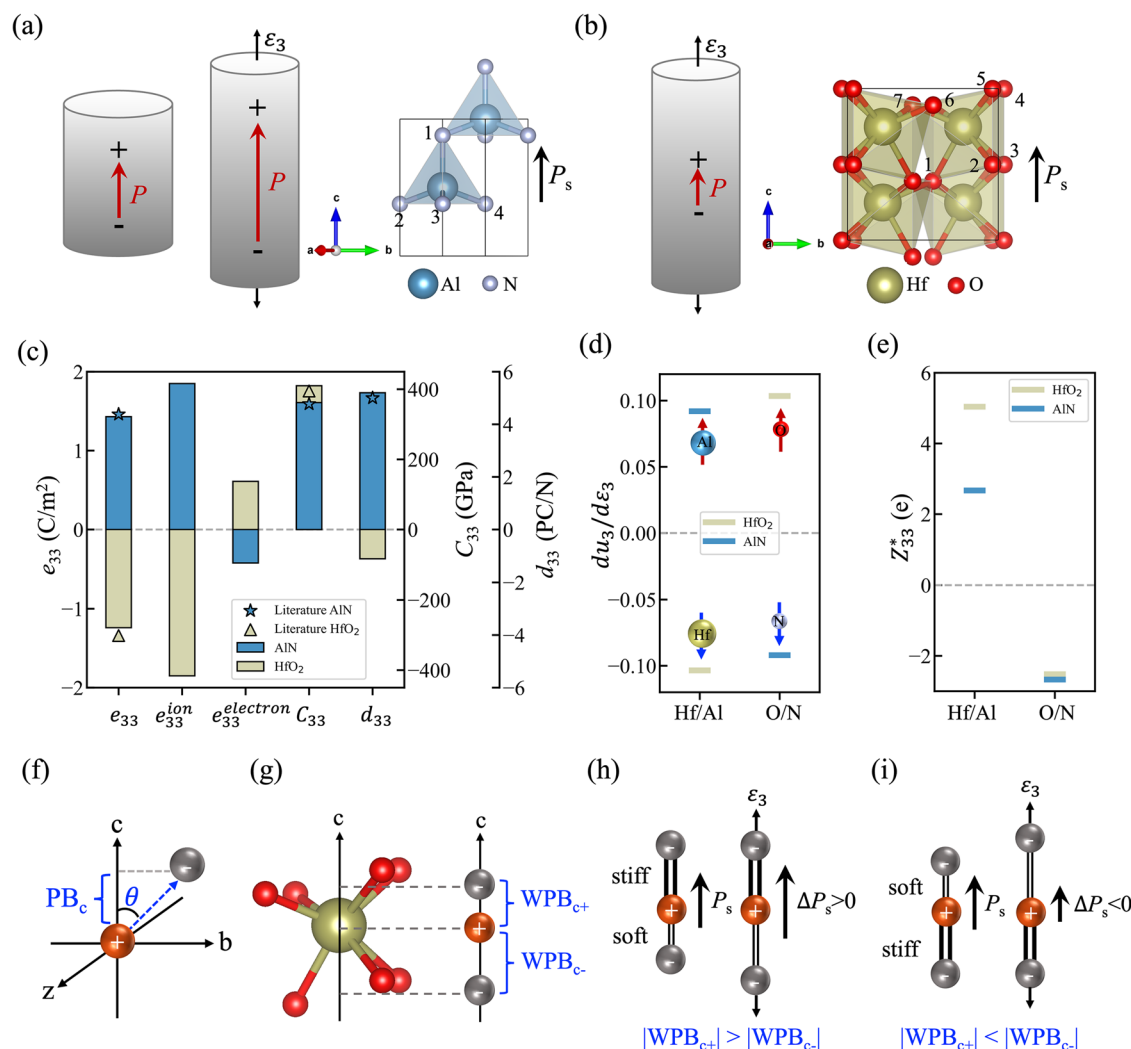


Fig. 1 | Negative piezoelectric response in HfO₂. Schematic diagrams of the **a** positive and **b** negative longitudinal piezoelectric effect, where the polarization increases and decreases with the tensile strain along the polar direction. In addition, the crystal structures of AlN and HfO₂ are provided with the numbers representing different nearest neighboring anions of the cation. **c** The piezoelectric coefficient e_{33} , $e_{33}^{electron}$, e_{33}^{ion} , d_{33} , and elastic constant C_{33} of HfO₂ and AlN. The data from

literatures^{25,29,30} are marked with stars or triangles. Factors of the ionic contribution for piezoelectric coefficient, **d** the atomic strain sensitivity du_3/de_3 and **e** the Born effective charge Z_{33}^* . Schematic diagrams describe the definition of **f** WPB_c , **g** WPB_{c+} and schematic draws for the mechanism responsible for the **h** positive piezoelectric effect and **i** negative piezoelectric effect.

the positive piezoelectric response was measured in La- and Y-doped HfO₂, while Dutta and his collaborators observed a negative piezoelectric response in La-doped HfO₂^{25,27,28}. They consider the difference may be caused by different textures of the sample caused by dopant. However, the effect of dopants on the piezoelectricity of hafnia has been little studied to date. Therefore, it is crucial to provide an intuitive and reasonable physical image to understand the intrinsic piezoelectric response of hafnia, while systematically exploring the influence of dopants on the longitudinal piezoelectric response.

In this study, a comprehensive exploration of the negative longitudinal piezoelectricity of hafnia and doped hafnia was undertaken based on density functional theory (DFT) calculations. An intuitive understanding of NLPE was first provided by introducing the asymmetric bonding stiffness along the strain direction, which is characterized quantitatively by weighted projected bond strength around cation in the *c* direction (WPB_c). Our finding indicates that the anti-parallel between WPB_c and bulk spontaneous polarization can result in the decrease of polarization with respect to tensile strain in the *c* direction, and thus a negative piezoelectricity. The influence of WPB_c on the piezoelectric effect of hafnia is further examined in 26 stability-screened doped hafnia. Our investigation confirms that the sign of the

piezoelectric coefficient is strongly dependent on the direction of the WPB_c with respect to the spontaneous polarization and suggests that the piezoelectric coefficient e_{33} could be evaluated by the average WPB_c and standard deviation (STD) of WPB_c .

Results and discussion

Understanding the NLPE from a quantitative DFT calculation and qualitative bonding environment analysis

To unlock the origin of NLPE in ferroelectric hafnia (*po*-HfO₂), the piezoelectric properties of AlN with positive longitudinal piezoelectric effect (PLPE) were calculated as a reference. As shown in Fig. 1b, the spontaneous polarization (P_s) of *po*-HfO₂ is caused by the off-centering of half of the oxygen anions within the unit cell with respect to the centrosymmetric cation sublattice, leading to a positive P_s in this unit cell. Additionally, each Hf atom is surrounded by seven nearest neighboring O atoms, and the bond lengths range from 2.04 to 2.27 Å. For AlN (Fig. 1a), the P_s is also positive and is attributed to the off-centering of the nitrogen anions concerning the centrosymmetric cation sublattice. Each Al atom is surrounded by four N atoms with similar bond lengths. The precise values of the bond length are provided in Supplementary

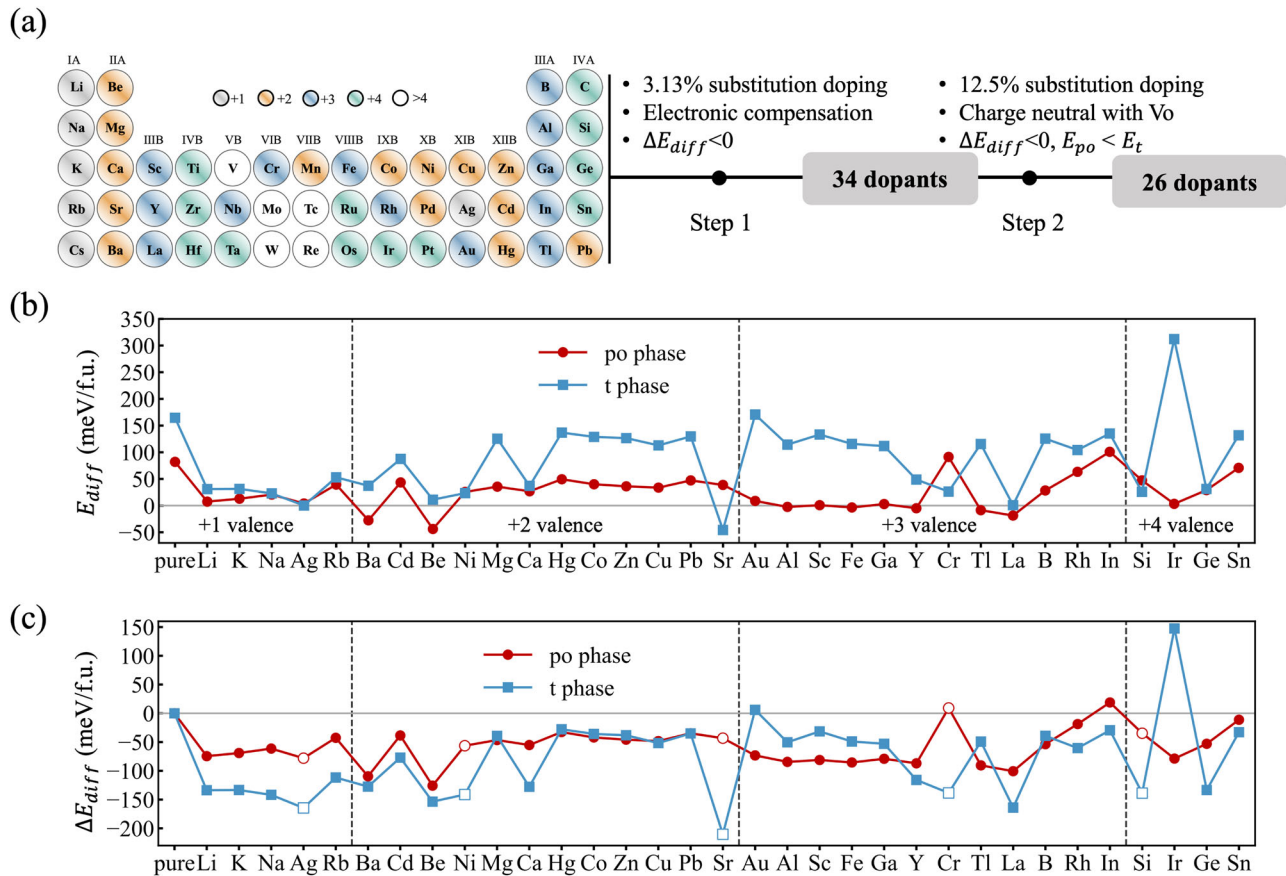


Fig. 2 | Phase stability screening of hafnia in the presence of various dopants. a Overall screening process and modeling conditions in each step. b Energy difference of the *po* phase and the *t* phase with respect to the *m* phase at 12.5% doping concentration, as computed using Eq. 2. c Relative energy difference between the

doped phases and pure phases at 12.5% doping concentration, as computed using Eq. 3. Dashed lines are employed to distinguish doping elements with different valence states. Hollow symbols in c represent that the energy of hafnia with these dopants is lower in the *t* phase compared to the *po* phase.

Tables 2 and 3. As shown in Fig. 1c, the calculated e_{33} of HfO_2 is -1.24 C/m^2 , which is similar to that of AlN (1.43 C/m^2) in magnitude but with an opposite sign. Moreover, the elastic constant C_{33} of HfO_2 is larger than that of AlN , induced by the strong ionic bond between Hf and O. Combining e_{ij} and C_{ij} , the piezoelectric strain coefficient (d_{33}) of HfO_2 has been determined to be a negative value but lower than that of AlN in magnitude. Our calculated results of AlN are in agreement with the previous DFT predictions^{29,30}. According to the definition of $d_{33} = \sum_{i=1}^6 e_{3i} (C^{-1})_{i3}$, contributions from the in-plane components of e_{31} and $(C^{-1})_{i3}$ need to be taken into account. Due to the larger and negative in-plane e_{31} and e_{32} of HfO_2 relative to that of AlN (Supplementary Table 13), the contribution of e_{33} is partially counteracted, which results in a relatively lower d_{33} of HfO_2 .

To illustrate the dominant factors of NLPE, different components contributing to e_{33} are discussed. The expression of e_{33} is given by

$$e_{33} = e_{33}^{\text{electron}} + e_{33}^{\text{ion}} = e_{33}^{\text{electron}} + \sum_k \frac{e}{ab} Z_{33}^*(k) \frac{du_3(k)}{d\epsilon_3} \quad (1)$$

The first term evaluates the contribution of electrons to the piezoelectric coefficient and is calculated with the ions fixed at their equilibrium fractional coordinates. The second term arises from the ionic contribution and measures the microscopic atomic displacements with respect to the strain. Here, a and b stand for the equilibrium lattice parameters, k represents each atom in the unit cell, Z_{33}^* is the Born effective charge and u_3 is the atomic coordinate along the c direction. It is clearly seen from Fig. 1c that in both systems, the ionic contribution dominates the total value of e_{33} , and the absolute value is almost the same

(1.85 C/m^2), but with the opposite sign. The electronic contribution of e_{33} in HfO_2 (0.61 C/m^2) is greater than that in AlN (-0.42 C/m^2), which leads to the magnitude of e_{33} for HfO_2 being slightly smaller than that of AlN . The calculated $du_3/d\epsilon_3$ and Z_{33}^* , as displayed in Fig. 1d, e, unambiguously demonstrate that the NLPE in hafnia is accompanied by the negative displacement of cations ($du_3/d\epsilon_3(\text{Hf}) < 0$) as well as the positive displacement of anions ($du_3/d\epsilon_3(\text{O}) > 0$) with respect to the tensile strain along c axis. This means that, in response to the macroscopic tensile strain along the c -axis, the cation center will move downward, while the anion center move upward. Due to the upward direction of P_s , this movement will yield a decrease of polarization and, thus, negative e_{33} . Conversely, for AlN with PLPE, the strain-induced atomic displacement for cations and anions are positive ($du_3/d\epsilon_3(\text{Al}) > 0$) and negative ($du_3/d\epsilon_3(\text{N}) < 0$), respectively, resulting in increased polarization and, thus, positive e_{33} . The Born effective charge Z_{33}^* for each atom is, in general, consistent with the nominal charge, but the value is greater than the nominal charge in HfO_2 , suggesting a blend of ionic and covalent bonds. Whereas in AlN , Z_{33}^* for each atom is smaller than its nominal charge, indicating a more pronounced covalent character³¹. Importantly, this nuance is not responsible for the opposite sign of the longitudinal piezoelectric effect in AlN and HfO_2 . This finding differs from the prior NLPE mechanism reported in van der Waals layered materials and hexagonal ABC ferroelectrics, where electronic contribution typically dominated due to their special stacking nature and interlayer bonding^{8,9,32}, and a detailed analysis can be found in Supplementary Note 1. In HfO_2 , due to the asymmetric but similar ionic/covalent bond properties on both sides of hafnium, atoms are more sensitive to the strain, resulting in a large $du/d\epsilon$. Combined with the large

effective charges of hafnium ($>5e$), the ionic contribution is dominated in HfO_2 .

The preceding discussion yields a quantitative conclusion that the NLPE is caused by the anomalous displacement of ions under strain. To offer a more intuitive understanding of the negative piezoelectricity of HfO_2 , its bonding environment is compared with AlN . Although previous studies have discussed the NLPE of HfO_2 from a bonding perspective, the correlation between the most longitudinal Hf-O bond and e_{33} has been discussed by overlooking other Hf-O bond contributions^{25,26}. Therefore, a rational and intuitive model needs to be established. Given our focus on the longitudinal piezoelectricity, we characterize the projected bond strength between cation and anion along the c direction (PB_c), as schematically shown in Fig. 1f. Centered around the cation, a positive PB_c represents the projection of its bonding with the anion is along the $+c$ direction, while a negative value indicates that the projected bond strength is in the $-c$ direction. Mapping in po -hafnia (Fig. 1g), each Hf is bonded with seven O anions with similar bond lengths, four bonds above the Hf cation showing positive PB_c and three bonds below Hf cation showing negative PB_c . We define the weighted PB_c (WPB_c) as the sum of all positive PB_c (WPB_{c+}) plus the sum of all the negative PB_c (WPB_{c-}) around a central cation. Due to the similar Hf-O bond lengths, the Hf-O_1 bond with the smallest longitudinal angle gives a stronger contribution to the WPB_{c-} , finally resulting in a negative WPB_c for Hf. The PB_c value for each Hf-O bond is listed in Supplementary Table 7. Therefore, in the structure with negative WPB_c , we can assume that a stiff bond is located below a soft bond along the c direction, as shown in Fig. 1i. When a tensile strain is applied along the c direction, it is evident that the soft bond will expansion easier than the stiff bond. Due to the anti-parallel direction between P_s and WPB_c , this expansion yields to a decrease of bulk polarization and a negative e_{33} .

In comparison, each Al in the AlN crystal structure is surrounded by four nearest neighbor N anions (Fig. 1a). Among them, the Al-N_1 bond, which is parallel to the c direction, gives a stronger contribution to the WPB_{c+} and leads to an overall positive WPB_c (see Supplementary Table 8 for detailed values). For the structure with positive WPB_c , it can be considered that a stiff bond is located above a soft bond along the c direction (Fig. 1h). Differing from HfO_2 , the WPB_c and P_s share the same direction in this case. As a consequence, with respect to the tensile strain in the c direction, the larger expansion of the soft bond will cause an increase in the bulk polarization, resulting in a positive e_{33} . The validation in other materials (PbTiO_3 , GeTe , and ZrO_2) can be found in Supplementary Fig. 2 and Tables 4–6, 9–12). In line with the above conclusion, when the direction of WPB_c is parallel to the spontaneous polarization (positive WPB_c), the e_{33} is positive. When the direction of WPB_c is antiparallel to the spontaneous polarization (negative WPB_c), the e_{33} is negative.

Stability screening in doped hafnia

In the above discussion, quantitative and qualitative explanations were provided to elucidate the origin of NLPE in hafnia. We first propose that the sign of the piezoelectric coefficient is intricately linked to the direction of the WPB_c with respect to the P_s . The primary contributor to the NLPE is identified as the opposing direction of these two vectors. Nevertheless, whether this conclusion is universal and how the value of WPB_c impacts the piezoelectric coefficient remains unclear. We address these questions through a systematic investigation of doped hafnia systems. Prior to calculating the piezoelectric coefficient, it is imperative to identify dopants that facilitate the formation of the po - HfO_2 phase. Earlier investigations have indicated that the po - HfO_2 is metastable^{23,33}. However, more recent studies have demonstrated that doping can effectively stabilize its ferroelectricity^{34–37}. To address the high computational cost associated with accurately modeling the effect of 49 dopants on the energetics of hafnia, a two-step screening process is performed³⁶, as illustrated in Fig. 2a. To ascertain the energy ordering of different phases of doped hafnia, the energy difference (E_{diff}) of the po phase and the t phase (the most stable phase at high temperature) with respect to the m phase (the most stable phase at

room temperature) is defined as

$$E_{\text{diff}} = E_{po(t)} - E_m \quad (2)$$

where $E_{po(t)}$ and E_m are the DFT energies of $po(t)$ and m phases, respectively. To emphasize the direct role of a dopant in the stabilization of the po and t phases, we further calculate the relative energy difference (ΔE_{diff}) between the doped phases and pure phases by

$$\Delta E_{\text{diff}} = E_{\text{diff}}^D - E_{\text{diff}}^{\text{pure}} \quad (3)$$

Here, a negative ΔE_{diff} represents that the dopant favors (or stabilizes) the po or t phase over the m phase more than the dopant-free pure case. Furthermore, if the energy of the po phase is lower than the energy of the t phase, one can anticipate that such dopants will enhance the ferroelectric behavior in hafnia.

In the first step, we investigated the influence of 49 dopants on the phase stability of po phase and m phase of hafnia. Based on previous findings^{36,38,39}, the energy difference between the po phase and the m phase has consistently exhibited a monotonic trend with doping concentration increase. Thus, to expedite the screening process while ensuring computational reliability, a 96-atom supercell with a 3.125% doping concentration is constructed for the po phase and the m phase through electron compensation (see details in method), we calculate the ΔE_{diff} using Eq. 3. Among them, 34 dopants with negative ΔE_{diff} for po phase are identified as favoring the ferroelectric phase and were further studied in step 2. In this step, we increase the sophistication of the model by introducing an appropriate oxygen vacancy to achieve charge neutrality and constraining the doping concentration at 12.5% for practical reasons. The number and arrangement of defects in the po , m and t phases are introduced in the method section. We found that the oxygen vacancies are energetically preferred in the vicinity of the dopants, especially for divalent element doping, and oxygen vacancy tends to occupy the O site with 3 Hf-O bonds, which is consistent with the findings of Batra et al.²³. The E_{diff} of the doped systems in Fig. 2b indicates that in most systems the m phase is still the most stable phase, consistent with the previous findings³⁶. However, compared to the undoped phase, the relative energy change of the po and t phases with respect to the m phase is significant. We plot the ΔE_{diff} in Fig. 2c to identify the dopants that can be expected as the promoters of the po phase³⁶. Among them, 27 out of 34 dopants favor the po phase. However, in the case of Rb, the relaxed structure exhibits significant distortion, and we exclude it for further analysis. The remaining 26 elements doped po - HfO_2 are selected for the study of piezoelectric properties. It is noteworthy that certain dopants predicted in our study, such as Y and La, have been experimentally identified to favor the ferroelectric phase⁴⁰.

Piezoelectric properties in doped hafnia

To the best of our knowledge, there has been little research into the piezoelectric coefficient of doped hafnia in previous works and even less research into how to control its piezoelectric coefficient. In our work, the piezoelectric coefficients of 26 doped po - HfO_2 are illustrated in Fig. 3a. Among them, Pb, Rh, and Sn demonstrate an active alloying effect on the enhancement of the piezoelectric coefficient e_{33} of hafnia, which equals to -1.72 C/m^2 , -1.33 C/m^2 , and -2.04 C/m^2 , respectively. Especially, the e_{33} value for Pb- and Sn-doped hafnia surpasses that of wurtzite AlN ^{29,30}, implying their substantial potential for electromechanical devices. Conversely, the remaining elements exhibit a weakening effect on the piezoelectric coefficient of hafnia, with eight elements (Au, Al, Sc, Fe, Ga, Y, Ge, Ir) doped hafnia even exhibiting sign reversal of piezoelectric coefficient or a positive piezoelectric response. As can be seen, the e_{33} of La- and Y-doped HfO_2 is almost zero. Therefore, in experiments, the sign of e_{33} in both systems is more susceptible to external stimuli, such as substrate strain and size effect, resulting in opposite signs. For example, the previous calculation has shown that epitaxial strain can change the sign of e_{33} of HfO_2 ²⁵. Here, we focus on the effect of elemental

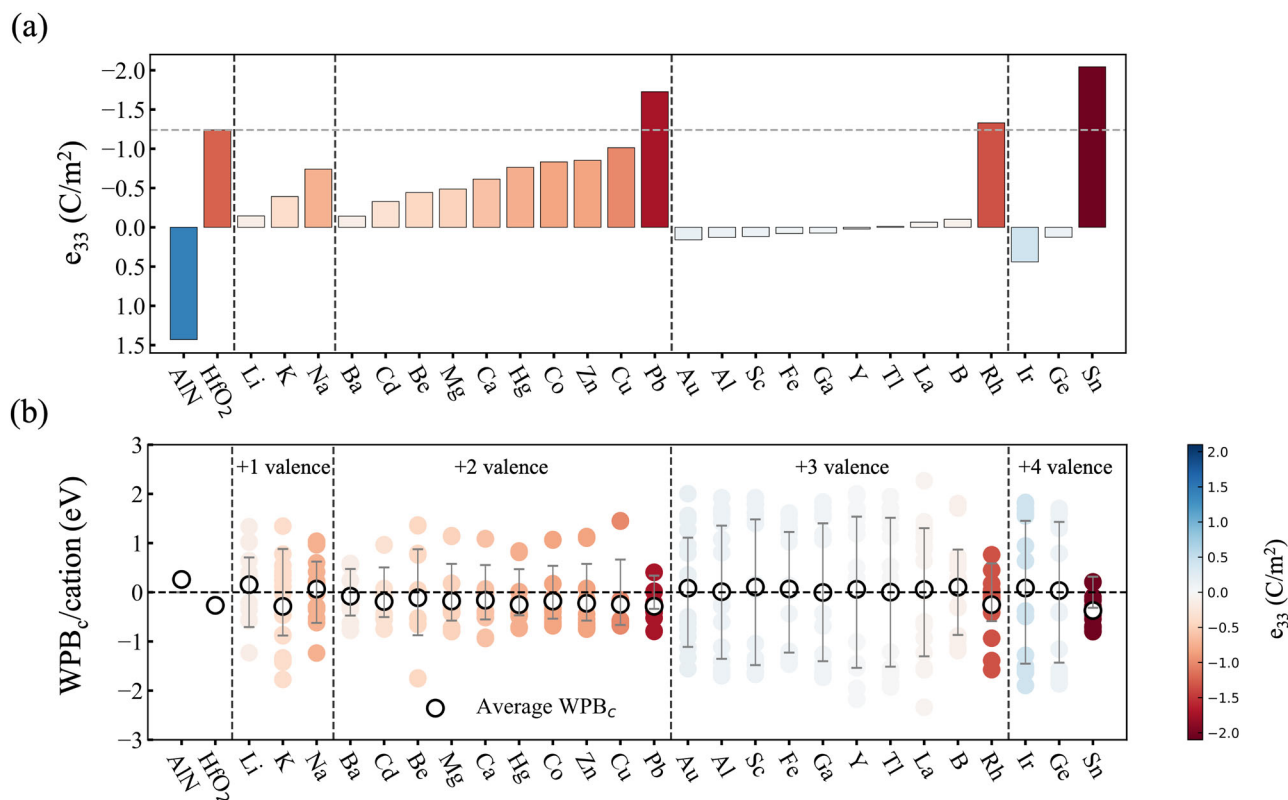


Fig. 3 | Piezoelectric response in doped hafnia. a Calculated e_{33} based on DFPT in selected doped systems. **b** The distribution of WPB_c of cations in the doped hafnia, a positive (negative) value represents the WPB_c is in the c ($-c$) direction. All error bars

shown in this figure represent \pm standard deviation and are based on counting statistics for each point. The wider the error bars, the larger the local bonding fluctuations of cations.

doping on piezoelectricity, while the influence of multi-factor will be investigated in future work.

Furthermore, to examine whether the sign of the piezoelectric coefficient is determined by the direction of WPB_c and to understand how the value of WPB_c influences the piezoelectric coefficient in doped hafnia, we conduct a meticulous study of the chemical bonding environment of cations. In contrast to undoped hafnia, the bonding environment around each cation differs in the doped systems, the distribution of WPB_c around all cations in each given system is depicted in Fig. 3b. It is evident that the WPB_c values vary significantly among different doping systems, with the systems exhibiting substantial fluctuations displaying relatively low e_{33} , particularly noticeable in the trivalent doped hafnia. As with undoped hafnia, to quantitatively characterize the direction and value of WPB_c of the doped systems, we employ the average WPB_c as a reference. From Fig. 3b, it is clear that there is a correlation between the sign of WPB_c and e_{33} , and most systems associated with negative WPB_c exhibit negative piezoelectric values. Additionally, there appears to be a discernible positive correlation between the average WPB_c value and the piezoelectric value. For instance, in Sn-doped hafnia with the most negative e_{33} , the average WPB_c is the lowest.

Here, we attempt to establish an intuitive correlation between WPB_c and e_{33} . The standard deviation (STD) of WPB_c is introduced to quantitatively measure local bonding fluctuations of cations, while the average WPB_c is employed to characterize the overall bonding direction and strength. The correlation between e_{33} and the bonding environment descriptors, STD-WPB_c and average WPB_c, are illustrated in Fig. 4a. The results clearly indicate that the more negative the average WPB_c and the smaller the standard deviation (STD) of WPB_c, the stronger the piezoelectric response. These observations align with the conclusions drawn from our analysis of pure hafnia. The introduction of the STD-WPB_c descriptor in the doping system reflects the structural distortion caused by defects, a largely distorted structure is also less responsive to changes in internal polarization

under strain⁴¹. These findings offer valuable insights for selecting suitable dopants when designing hafnia with enhanced piezoelectric or ferroelectric performance. For instance, choosing dopants with an ionic radius similar to Hf⁴⁺ appears to reduce local bonding fluctuations. Additionally, selecting dopants with lower electronegativity than hafnia can enhance bond strength between dopants and oxygen⁴², potentially resulting in a larger average WPB_c.

Finally, to provide experimenters with more intuitive information, we calculate the elastic constant C_{33} and piezoelectric strain coefficient d_{33} of Pb₂Hf₁₄O₃₀, Sn₂Hf₁₄O₃₂, and Rh₂Hf₁₄O₃₁, as shown in Fig. 4b. A complete result of elastic tensors and piezoelectric tensors are presented in the Supplementary Tables 14–15. In comparison to pure HfO₂, the elastic constants of all three systems have decreased. However, these values remain higher than 300 GPa, which indicates reliable mechanical strength. Combining e_{ij} and C_{ij} , we calculate the d_{33} . Among them, the d_{33} of the Pb-doped system slightly decreases compared to that in pure hafnia, while the Sn- and Rh-doped systems show more than two times enhancement. Especially, the d_{33} of Sn-doped HfO₂ is about 3.8 pC/N, comparable to that of AlN. In addition, the calculated spontaneous polarization of Sn_{0.125}Hf_{0.875}O₂ is 0.54 C/m², which is similar to that previously reported spontaneous polarization of pure HfO₂ (0.52–0.54 C/m²)^{25,43}. Considering that the stability of the po phase of Sn_{0.125}Hf_{0.875}O₂ is better than that of the pure phase, the possibility of polarization switching could make Sn_{0.125}Hf_{0.875}O₂ a promising candidate for ferroelectricity. According to the result, we encourage more experimental trials to further explore the piezoelectric properties of similar compounds.

In this work, we carried out an extensive investigation on the negative longitudinal piezoelectricity from both quantitative DFT calculation and qualitative bonding environment analysis. From the computational results, this counterintuitive piezoelectric effect stemming from the negative ionic contribution of e_{33} , facilitated by the reverse strain displacement of cations

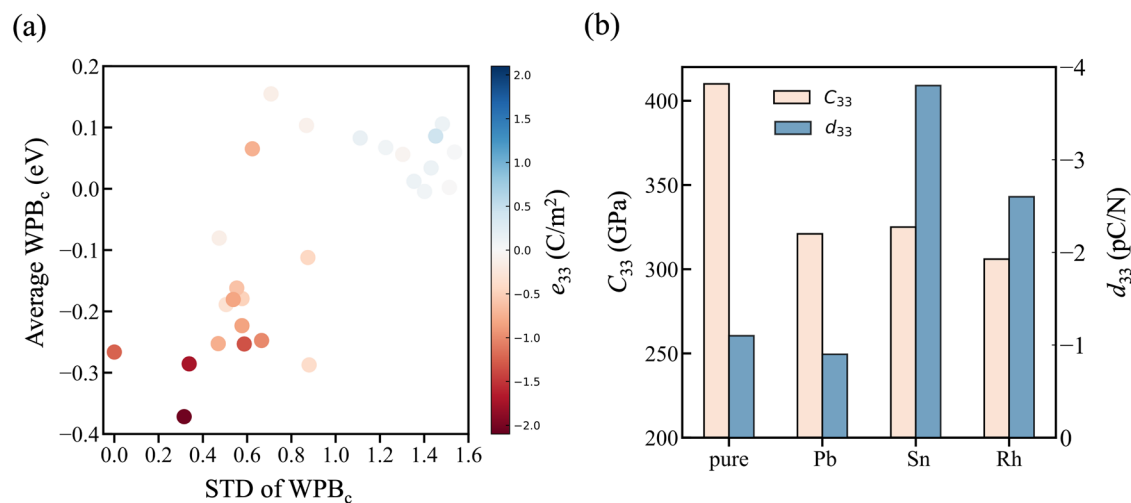


Fig. 4 | Impact of bonding environment on e_{33} and promising candidates. **a** Piezoelectric coefficient e_{33} distribution versus the average WPB_c and the standard deviation of WPB_c. Among them, three doped hafnia systems (Pb-, Sn-, Rh-) with e_{33}

greater than pure hafnia are selected for further simulations for **b** the elastic constant C_{33} and piezoelectric coefficient d_{33} .

and anions compared to the positive piezoelectric materials. Furthermore, the weighted projected bond strength along the c direction (WPB_c) is first proposed to quantitatively characterize the asymmetric bonding stiffness along the strain direction. Our finding indicates that the direction of WPB_c with respect to spontaneous polarization is the essential reason for the sign of the longitudinal piezoelectric coefficient. Further meticulous study on the chemical bonding environment of cations in doped hafnia confirms the relationship between WPB_c and e_{33} . It is found that the sign of the piezoelectric coefficient is strongly dependent on the direction of the WPB_c with respect to the spontaneous polarization, a more negative average WPB_c and a lower standard deviation (STD) of WPB_c can lead to a stronger piezoelectric response. Importantly, the Sn-doped hafnia with the lowest value of average WPB_c and STD-WPB_c is identified to have the highest piezoelectric coefficient (-2.04 C/m²) compared to other dopants. We hope this work could inspire future computational and experimental studies in the understanding of the piezoelectric effect. In addition, these insights can be used to discover new choices for next-generation electromechanical devices.

Methods

DFT calculations

In this work, all calculations based on density functional theory (DFT) were performed within the Vienna Ab initio Simulation Package (VASP), using the projector augmented-wave (PAW) method^{44,45}. The wave functions were expanded in a plane-wave basis set with an energy cutoff of 520 eV. The exchange-correlation interaction was treated within the generalized gradient approximation (GGA) in the form of Perdew–Burke–Ernzerhof (PBE) format⁴⁶. The convergence criteria were set to 10^{-6} eV for total energy and 0.01 eV/Å for the force on each atom. In the DFT calculations, the Γ -centered k -point meshes were adopted. For the supercell with 96 atoms, a $3 \times 3 \times 3$ k mesh was chosen for polar orthorhombic (po) and monoclinic (m) phases. For supercell with 48 atoms, $3 \times 3 \times 6$ k mesh was chosen for po and m phases, and $4 \times 4 \times 3$ k mesh for the tetragonal (t) phase, respectively. The piezoelectric stress coefficients were calculated by using the preset workflow based on density functional perturbation theory (DFPT), while the elastic tensors were computed by the workflow that fits the strain-stress relationship by performing six independent components of Green–Lagrange strain tensor with four magnitudes ($\pm 0.5\%$, $\pm 1\%$) for the original structure^{47,48}. Bonding strengths were obtained by the crystal orbital Hamiltonian population (COHP) method, which is implemented in the LOBSTER code⁴⁹.

Construction of doped hafnia models

For isovalent dopants replacing Hf, the systems maintain charge neutrality. For aliovalent dopants, at 3.125% doping concentration, electron compensation is applied to the 96-atom supercell to accelerate the screening process, where a single dopant substituting an Hf atom and the charge is electronically compensated. At 12.5% doping concentration, various numbers of oxygen vacancies (V_o) were introduced for charge compensation. Specifically, substituting every two Hf with +1 valence state dopants is accompanied by the removal of three V_o , similarly, with +2 and +3 valence state dopants require the removal of two and one V_o , respectively, this approach has been widely utilized to construct the ferroelectric HfO₂ defect structure^{36,38,39}. The defects, such as doping element and V_o were arranged in supercells with 48 atoms based on low electrostatic energy criteria, as implemented in the Python Material Genomics (pymatgen) code⁵⁰. Considering the large number of possible arrangements of defects ($>10^4$, for dopants with +1 valence state), the configurations were sorted in sequence with the electrostatic energy, and then six configurations with the lowest electrostatic energy were selected and relaxed with DFT calculations⁵¹. The configuration with the lowest energy was then chosen as a representative of each valence state and proceeded with DFPT calculations. The position arrangement of the defects in doped hafnia systems is shown in Supplementary Fig. 3.

Data availability

All relevant data are included in the manuscript and the supplementary information file. Additional data are available from the authors upon reasonable request.

Received: 14 March 2024; Accepted: 5 July 2024;

Published online: 22 July 2024

References

- Curie, J. & Curie, P. Développement par compression de l'électricité polaire dans les cristaux hémihédres à faces inclinées. *Bull. Minéral.* **3**, 90–93 (1880).
- Chorsi, M. T. et al. Piezoelectric biomaterials for sensors and actuators. *Adv. Mater.* **31**, 1802084 (2019).
- Qiu, Y. et al. Piezoelectric micromachined ultrasound transducer (PMUT) arrays for integrated sensing, actuation and imaging. *Sensors* **15**, 8020–8041 (2015).

4. Dong, K., Peng, X. & Wang, Z. L. Fiber/fabric-based piezoelectric and triboelectric nanogenerators for flexible/stretchable and wearable electronics and artificial intelligence. *Adv. Mater.* **32**, 1902549 (2020).
5. Scott, J. Applications of modern ferroelectrics. *Science* **315**, 954–959 (2007).
6. Katsouras, I. et al. The negative piezoelectric effect of the ferroelectric polymer poly (vinylidene fluoride). *Nat. Mater.* **15**, 78–84 (2016).
7. Bystrov, V. S. et al. Molecular modeling of the piezoelectric effect in the ferroelectric polymer poly (vinylidene fluoride)(PVDF). *J. Mol. Model.* **19**, 3591–3602 (2013).
8. You, L. et al. Origin of giant negative piezoelectricity in a layered van der Waals ferroelectric. *Sci. Adv.* **5**, eaav3780 (2019).
9. Liu, S. & Cohen, R. Origin of negative longitudinal piezoelectric effect. *Phys. Rev. Lett.* **119**, 207601 (2017).
10. Arora, A., Rawat, A. & De Sarkar, A. Negative piezoelectricity and enhanced electrical conductivity at the interfaces of two-dimensional dialkali oxide and chalcogenide monolayers. *Phys. Rev. B* **107**, 085402 (2023).
11. Kim, J., Rabe, K. M. & Vanderbilt, D. Negative piezoelectric response of van der Waals layered bismuth tellurohalides. *Phys. Rev. B* **100**, 104115 (2019).
12. Zhang, S., Xia, R., Shrouf, T. R., Zang, G. & Wang, J. Characterization of lead free (K_{0.5}Na_{0.5})NbO₃–LiSbO₃ piezoceramic. *Solid State Commun.* **141**, 675–679 (2007).
13. Börscke, T., Müller, J., Bräuhäus, D., Schröder, U. & Böttger, U. Ferroelectricity in hafnium oxide thin films. *Appl. Phys. Lett.* **99**, 102903 (2011).
14. Müller, J. et al. Ferroelectric Zr_{0.5}Hf_{0.5}O₂ thin films for nonvolatile memory applications. *Appl. Phys. Lett.* **99**, 112901 (2011).
15. Müller, J. et al. Ferroelectricity in yttrium-doped hafnium oxide. *J. Appl. Phys.* **110**, 114113 (2011).
16. Schroeder, U. et al. Lanthanum-doped hafnium oxide: a robust ferroelectric material. *Inorg. Chem.* **57**, 2752–2765 (2018).
17. Peng, R. C. et al. Revealing the role of spacer layer in domain dynamics of Hf_{0.5}Zr_{0.5}O₂ thin films for ferroelectrics. *Adv. Funct. Mater.* **2403864**, 1 (2024).
18. Xu, X. et al. Kinetically stabilized ferroelectricity in bulk single-crystalline HfO₂. *Nat. Mater.* **20**, 826–832 (2021).
19. Sang, X., Grimley, E. D., Schenk, T., Schroeder, U. & LeBeau, J. M. On the structural origins of ferroelectricity in HfO₂ thin films. *Appl. Phys. Lett.* **106**, 162905 (2015).
20. Müller, J. et al. Ferroelectricity in simple binary ZrO₂ and HfO₂. *Nano Lett.* **12**, 4318–4323 (2012).
21. Hyuk Park, M. et al. Effect of forming gas annealing on the ferroelectric properties of Hf_{0.5}Zr_{0.5}O₂ thin films with and without Pt electrodes. *Appl. Phys. Lett.* **102**, 112914 (2013).
22. Polakowski, P. & Müller, J. Ferroelectricity in undoped hafnium oxide. *Appl. Phys. Lett.* **106**, 232905 (2015).
23. Batra, R., Tran, H. D. & Ramprasad, R. Stabilization of metastable phases in hafnia owing to surface energy effects. *Appl. Phys. Lett.* **108**, 172902 (2016).
24. Beyer, S. et al. in 2020 IEEE International Memory Workshop (IMW). 1–4 (IEEE).
25. Dutta, S. et al. Piezoelectricity in hafnia. *Nat. Commun.* **12**, 7301 (2021).
26. Liu, J., Liu, S., Yang, J.-Y. & Liu, L. Electric auxetic effect in piezoelectrics. *Phys. Rev. Lett.* **125**, 197601 (2020).
27. Schenk, T. et al. Toward thick piezoelectric HfO₂-based films. *Phys. Status Solidi* **14**, 1900626 (2020).
28. Starschich, S., Griesche, D., Schneller, T., Waser, R. & Böttger, U. Chemical solution deposition of ferroelectric yttrium-doped hafnium oxide films on platinum electrodes. *Appl. Phys. Lett.* **104**, 202903 (2014).
29. Jing, H. et al. Large piezoelectric and elastic properties in B and Sc codoped wurtzite AlN. *J. Appl. Phys.* **131**, 245108 (2022).
30. Noor-A-Alam, M., Olszewski, O. Z., Campanella, H. & Nolan, M. Large piezoelectric response and ferroelectricity in Li and V/Nb/Ta co-doped w-AlN. *ACS Appl. Mater. Interfaces* **13**, 944–954 (2021).
31. Błoński, P. & Łodziana, Z. Correlation between the ionic potential and thermal stability of metal borohydrides: first-principles investigations. *Phys. Rev. B* **90**, 054114 (2014).
32. Qi, Y. & Rappe, A. M. Widespread negative longitudinal piezoelectric responses in ferroelectric crystals with layered structures. *Phys. Rev. Lett.* **126**, 217601 (2021).
33. Ohtaka, O. et al. Phase relations and volume changes of hafnia under high pressure and high temperature. *J. Am. Ceram. Soc.* **84**, 1369–1373 (2001).
34. Müller, S. et al. Ferroelectricity in Gd-doped HfO₂ thin films. *ECS J. Solid State Sci. Technol.* **1**, N123 (2012).
35. Müller, S. et al. Incipient ferroelectricity in Al-doped HfO₂ thin films. *Adv. Funct. Mater.* **22**, 2412–2417 (2012).
36. Batra, R., Huan, T. D., Rossetti, J. G. A. & Ramprasad, R. Dopants promoting ferroelectricity in hafnia: insights from a comprehensive chemical space exploration. *Chem. Mater.* **29**, 9102–9109 (2017).
37. Starschich, S. & Boettger, U. An extensive study of the influence of dopants on the ferroelectric properties of HfO₂. *J. Mater. Chem. C* **5**, 333–338 (2017).
38. Falkowski, M., Künneth, C., Materlik, R. & Kersch, A. Unexpectedly large energy variations from dopant interactions in ferroelectric HfO₂ from high-throughput ab initio calculations. *npj Comput. Mater.* **4**, 73 (2018).
39. Materlik, R., Künneth, C., Falkowski, M., Mikolajick, T. & Kersch, A. Al-, Y-, and La-doping effects favoring intrinsic and field induced ferroelectricity in HfO₂: a first principles study. *J. Appl. Phys.* **123**, 164101 (2018).
40. Schroeder, U., Hwang, C. S. & Funakubo, H. *Ferroelectricity in Doped Hafnium Oxide: Materials, Properties and Devices*. (Woodhead Publishing, 2019).
41. Tholander, C., Abrikosov, I. A., Hultman, L. & Tasnádi, F. Volume matching condition to establish the enhanced piezoelectricity in ternary (Sc,Y)_{0.5}(Al,Ga,In)_{0.5}N alloys. *Phys. Rev. B* **87**, 094107 (2013).
42. Moltved, K. A. & Kepp, K. P. The chemical bond between transition metals and oxygen: electronegativity, d-orbital effects, and oxophilicity as descriptors of metal–oxygen interactions. *J. Phys. Chem. C* **123**, 18432–18444 (2019).
43. Huan, T. D., Sharma, V., Rossetti, G. A. Jr & Ramprasad, R. Pathways towards ferroelectricity in hafnia. *Phys. Rev. B* **90**, 064111 (2014).
44. Kresse, G. & Furthmüller, J. Efficient iterative schemes for ab initio total-energy calculations using a plane-wave basis set. *Phys. Rev. B* **54**, 11169 (1996).
45. Kresse, G. & Furthmüller, J. Efficiency of ab-initio total energy calculations for metals and semiconductors using a plane-wave basis set. *Comput. Mater. Sci.* **6**, 15–50 (1996).
46. Perdew, J. P., Burke, K. E. & Ernzerhof, M. Generalized gradient approximation made simple. *Phys. Rev. Lett.* **77**, 3865–3868 (1997).
47. De Jong, M. et al. Charting the complete elastic properties of inorganic crystalline compounds. *Sci. Data* **2**, 1–13 (2015).
48. Wu, X., Vanderbilt, D. & Hamann, D. Systematic treatment of displacements, strains, and electric fields in density-functional perturbation theory. *Phys. Rev. B* **72**, 035105 (2005).
49. Maintz, S., Deringer, V. L., Tchougreeff, A. L. & Dronskowski, R. LOBSTER: a tool to extract chemical bonding from plane-wave based DFT. *J. Comput. Chem.* **37**, 1030–1035 (2016).
50. Ong, S. P. et al. Python Materials Genomics (pymatgen): a robust, open-source Python library for materials analysis. *Comput. Mater. Sci.* **68**, 314–319 (2013).
51. Miara, L. J. et al. Effect of Rb and Ta doping on the ionic conductivity and stability of the garnet Li_{7+2x-y}(La_{3-x}Rb_x)(Zr_{2-y}Ta_y)O₁₂ (0 ≤ x ≤ 0.375, 0 ≤ y ≤ 1) superionic conductor: a first principles investigation. *Chem. Mater.* **25**, 3048–3055 (2013).

Acknowledgements

This work was supported by the National Natural Science Foundation of China (52072240) and the Shanghai Technology Innovation Action Plan 2020-Integrated Circuit Technology Support Program (Project No. 20DZ1100603). All simulations were carried out with computational resources from Shanghai Jiao Tong University High Performance Computing Center.

Author contributions

H.J. designed this work, performed the DFT calculations, and wrote the paper; C.G. discussed the methodology; H.Z. guided this research. All authors discussed and commented on the paper.

Competing interests

The authors declare no competing interest.

Additional information

Supplementary information The online version contains supplementary material available at <https://doi.org/10.1038/s41524-024-01354-y>.

Correspondence and requests for materials should be addressed to Hong Zhu.

Reprints and permissions information is available at <http://www.nature.com/reprints>

Publisher's note Springer Nature remains neutral with regard to jurisdictional claims in published maps and institutional affiliations.

Open Access This article is licensed under a Creative Commons Attribution 4.0 International License, which permits use, sharing, adaptation, distribution and reproduction in any medium or format, as long as you give appropriate credit to the original author(s) and the source, provide a link to the Creative Commons licence, and indicate if changes were made. The images or other third party material in this article are included in the article's Creative Commons licence, unless indicated otherwise in a credit line to the material. If material is not included in the article's Creative Commons licence and your intended use is not permitted by statutory regulation or exceeds the permitted use, you will need to obtain permission directly from the copyright holder. To view a copy of this licence, visit <http://creativecommons.org/licenses/by/4.0/>.

© The Author(s) 2024